Model Predictive Control of Multilevel CHB STATCOM in Wind Farm Application Using Diophantine Equations

Mohammad Reza Nasiri, Shahrokh Farhangi, *Member, IEEE,*
and José Rodríguez, *Fellow, IEEE*

***Abstract*—The Finite Control Set Model Predictive Control (FCS-MPC) for power electronic converters, provides high dynamic performance, based on the limited number of inputs and accurate model of the converter. By applying this algorithm to multilevel converters such as Cascaded H-Bridge based STATic var COMpensator (CHB STATCOM), the dynamic performance is degraded, because the optimized input is achieved by searching among a large set of switching combinations and redundancies. This paper proposes an FCS-MPC algorithm, which benefits high dynamic performance for the CHB STATCOM, despite the large set of inputs. The proposed FCS-MPC replaces the time-consuming optimization algorithm by solving Diophantine equations over the large set of switching combinations. The desired switching combination and all its redundancies are determined in a minimum execution time. The proposed FCS-MPC performance is validated by applying to two configurations: 1) a 15-level CHB STATCOM with energy storage capability for a short-term active power smoothing and reactive power compensation of a 10 MW fixed speed wind farm at medium voltage, and 2) an experimental 7-level CHB STATCOM at low voltage.**

***Index Terms*—Model predictive control, CHB STATCOM, Diophantine equations, wind farm.**

I. Introduction

Multilevel STATCOMs are an efficient alternative to the two-level ones, providing transformerless high voltage compensator, low harmonic currents, high quality voltage, and low Electro Magnetic Interference in the medium voltage level applications. One of the well-known and attractive multilevel STATCOM topologies is the Cascaded H-Bridge (CHB) STATCOM, due to an excellent modularity in the CHB configuration [1, 2]. CHB STATCOM, based on the series connection of H-bridges provides the required output voltage level. The CHB converter with equal dc link voltages, has many redundancies for the switching combinations to provide the same output voltage. The redundancies is used for dc links voltage balancing, reducing switching losses, and decreasing common mode voltage [3, 4].

Various classical linear control approaches and modulation techniques are proposed for the CHB STATCOM [5-7]. Recently, Model Predictive Control (MPC) has received more attention in the power converters control. The advantages of MPC such as high dynamic performance, suitability for nonlinear and constrained systems, multi-objective capabilities [8], as well as, its simplicity and intuitiveness make it a powerful control strategy in power electronics [9].

The MPC algorithms are classified into two groups of integer or continuous optimization problem [10]. Continuous Control Set MPC (CCS-MPC) uses a modulator to synthesize the control action applicable to the power converter. The CCS-MPC strategies, such as Generalized Predictive Control (GPC) and Explicit MPC (EMPC), present the MPC problem with complex formulations, but they have less computational cost because they compute a part or all of the optimization problems offline. For this reason, they can address long prediction horizon problems. If the constraints are included in the GPC method, the optimization has to be computed by more computationally taxing numerical algorithms [10, 11].

The Finite Control Set MPC (FCS-MPC) uses the advantage of a limited number of switching combinations in a power converter to solve the optimization problem. A discrete converter model with integer control signals is used to predict the system behavior for any permissible actuation sequence, up to the prediction horizon. The actuation sequence that minimizes a cost function is selected, and its first switching action is applied to the converter at the next sampling time [12]. Main advantage of FCS-MPC relies on direct application of the control action to the converter, without requiring a modulation stage [13, 14]. The FCS-MPC is capable of improving converter parameters, such as switching losses and the common mode voltage.

In the FSC-MPC, the optimization problem is solved online in a loop. Therefore, it is limited to lower prediction horizons due to online computational cost [10]. In the FSC-MPC with control horizon one, the optimal control action should be applied at the same sampling time k. However, due to online optimization delay, it is applied at the start of the next sampling time $k+1$, affecting the converter performance

Manuscript received July 26, 2017; revised February 28, 2018; accepted April 16, 2018.

M. R. Nasiri and S. Farhangi are with the School of Electrical and Computer Engineering, University of Tehran, Tehran, Iran (e-mail: mrnasiri2003@ut.ac.ir; farhangi@ut.ac.ir).

J. Rodríguez is with the Universidad Andres Bello, Santiago, Chile (e-mail: jose.rodriguez@unab.cl).

significantly [10, 15]. This digital delay problem is resolved by optimizing the cost function for the predicted variables at sampling time $k+2$ (with tolerance of higher predictive approximation), leading to an optimized control action applicable at the start of the sampling time $k+1$ [9, 10, 15].

The FCS-MPC algorithm with horizon one (hereafter briefly MPC in this study) is used to control of electronic power converters, featuring high dynamic performance, intuitiveness, simplicity without employing any modulation scheme [9, 14]. The MPC has been used to achieve different control objectives in power electronic converter [16-18]. It could be effectively applied to two-level, three-level converters and AC/AC matrix converter due to a small set of inputs [15, 19, 20]. In the multilevel symmetrical converters, with a large set of switching combinations and redundancies, the number of iterations for online optimization loop is significantly increased. In the CHB converters with N cells per phase, the optimal current (voltage) vector is searched between $(2N+1)^3$ three-phase switching combinations (states), and $2^{N+1}-1$ phase switching combinations in each of the phases [21]. Most of these switching combinations are redundant and do not change the output vector. By increasing the voltage levels, it is difficult to implement the control algorithm using standard signal processors [22]. In [22], for each voltage vector, only one of the three-phase switching redundancies is considered, and it improves the speed of optimization by limiting the search subspace to seven vectors adjacent to the previously applied vector. In [21], a hybrid design, integrating dead-beat control, MPC, and PWM is proposed for a 19-level CHB STATCOM. A cost function is used for the voltage balancing and reducing the number of transitions within the HB cells using phase redundancies. The transition is the change of a cell mode between 1, 0 or 0, -1, which increases switching losses. The MPC in the best condition, for a 28% reduction of transitions, increases the dc links voltage ripple up to 103%, which affects output current quality of the converter. This relatively complicated control system has been experimentally implemented with parallel processing method on a platform with four processors.

The authors in [23], divided the MPC optimization problem into two sub optimization of current control and voltage balancing in a CHB STATCOM. The current control MPC, uses Dynamic Programming search method in order to find the optimal voltage vector and sends it to the voltage balancing MPC. In the voltage balancing MPC, a cost function is defined for the dc link voltage balancing and reducing the number of transitions. Authors in [24] improved the method of [23], using the search algorithm branch and bound in the current control MPC. A seven-level CHB STATCOM has been implemented experimentally using the MPC control method in [24]. The control platform consists of a DSP, an FPGA two external ADCs for measuring AC signals, and nine slave controllers. The total execution time of measuring data and executing MPC code in each sample time is approximately close to the sampling period in this control platform. Therefore, it requires more powerful processors and parallel processing methods, for the converters with higher voltage levels. Furthermore, the ripple of dc link voltage is about 27% peak to peak, which is relatively large. Its performance in reducing the number of transitions has not been reported.

This paper proposes a fast MPC method for CHB STATCOM with any number of HB cells. Despite the large number of switching combinations and redundancies, this control method has a very small execution time, so that there is no need to resolve aforementioned MPC digital delay. In addition, the controller output directly determines the optimal switching combination without employing any modulation scheme. The control system can be easily implemented with a standard processor without requiring parallel processing.

The proposed MPC, eliminates the optimization loop by solving a Diophantine equations system [25, 26] over a large set of switching combinations, obtained by direct solution of cost function and system model. The optimal three-phase switching combination and its redundancies in each sample time are provided at the same time. The redundancies are generated simply by changing an integer variable, therefore, in a multilevel converter, they can be easily optimized for various purposes, such as reducing switching losses, reducing common mode voltage or both, or another objective function. The main purpose of using phase redundancies is to balance the dc links voltage of that phase. The use of MPC for the dc links voltage balancing and reducing switching losses, posses some disadvantages discussed during the review of the previous articles. In this paper, a simple sorting method is used for the voltage balancing of dc links in each phase. After selecting some cells by sorting to be in mode 1 or -1, it is possible to replace some of the selected cells with non-selected (mode 0) cells, by considering different conditions to reduce switching losses. Considering the different conditions for each cell is a Boolean algebra problem that works very fast. Sorting the dc links voltage up to 10 cells, takes about $1.1\,\mu s$ with the processor used in this research, which is negligible compared to the sampling time.

Since the focus of this paper is on the application of Diophantine equations in the current-control MPC. Therefore, the method in its simplest case will be considered by choosing the middle switching redundancy of Diophantine solution, and implementing a simple sort without reducing the switching losses. The proposed MPC controller is validated in two steps: 1) it is applied to a 15-level CHB STATCOM with Energy Storage Capability (ESC) for a short-term active power smoothing and reactive power compensation of a 10 MW, 20kV wind farm, 2) experimental results of a 7-level CHB STATCOM at 380 V is also investigated.

II. SYMMETRIC CHB STATCOM

The symmetric CHB STATCOM is a shunt modular compensator at the medium voltage level. The configuration of a multilevel CHB STATCOM is shown in Fig. 1. Due to excellent modularity, in the case of a fault in one cell, the faulty cell can be easily replaced. Furthermore, it is possible to bypass the faulty cell without stopping the compensator, providing nearly continuous overhaul accessibility.

This article has been accepted for publication in a future issue of this journal, but has not been fully edited. Content may change prior to final publication. Citation information: DOI 10.1109/TIE.2018.2833055, IEEE Transactions on Industrial Electronics

In the symmetric CHB STATCOM with N cells per phase, the number of output voltage levels is equal to $l = 2N + 1$. Number of all possible switching combinations (states) is l^3, and the number of switching redundancies is equal to $(l-1)^3$. For example, in the 15-level and 7-level CHB converters, there are 3375 switching combinations, 2744 redundancies and 343 switching combinations, 216 redundancies, respectively [27].

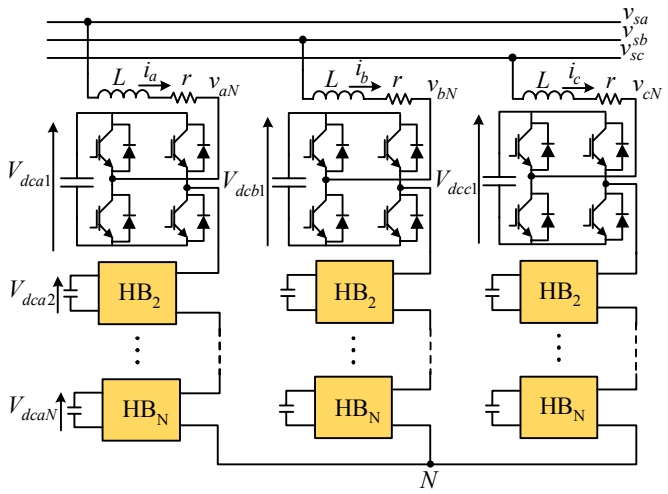

Fig. 1. Transformerless N-cell CHB STATCOM.

III. Model Predictive Control Algorithm

The basic MPC algorithm in each sample time k, begins with measuring the state variables $\boldsymbol{x}(k)$ and disturbances $\boldsymbol{d}(k)$ of the system. By using these values, discrete model of the system is utilized to predict the next state variables $\boldsymbol{x}(k+1)$ for each possible input $\boldsymbol{u}$. A cost function J is optimized in a loop over the predicted state variables and next references $\boldsymbol{x}^*(k+1)$. The possible input $\boldsymbol{u}^*$ with minimum cost is applied in the next sample time $k+1$ [28, 29], i.e.

$$\boldsymbol{u}(k+1) = \boldsymbol{u}^* \tag{1}$$

The algorithm is depicted in Fig. 2 (a). The optimization loop will be time-consuming for a large set of inputs.

To address the digital delay, the cost function should be optimized for the state variables $\boldsymbol{x}(k+2)$ and the references $\boldsymbol{x}^*(k+2)$ instead of $\boldsymbol{x}(k+1)$ and $\boldsymbol{x}^*(k+1)$ [10].

IV. Proposed Model Predictive Control Algorithm

The main problem of MPC when applied to the symmetrical CHB converters, is the high number of switching combinations that must be evaluated in the optimization loop [30]. The time-consuming optimization loop can be eliminated by direct solution of the system model and solving a system of Diophantine equations over the set of switching combinations.

A. Converter Model

Fig. 1 shows the topology of a multilevel CHB STATCOM connected to the grid. The phase to neutral voltages of each phase are given by:

$$\begin{bmatrix} v_{aN} \\ v_{bN} \\ v_{cN} \end{bmatrix} = \begin{bmatrix} s_a \\ s_b \\ s_c \end{bmatrix} V_{dc} \tag{2}$$

where V_{dc} is the dc link voltage, and $[s_a\ s_b\ s_c]^T$ is the switching combination (state) of phases a,b and c, and its elements are integer values bounded in $[-N, N]$, where the superscript ^{T} denotes the transpose of the vector. The output space vector generated by the converter is defined as [27]:

$$\boldsymbol{V_c} = \sqrt{\frac{2}{3}}(\mathrm{v_{aN}} + \boldsymbol{a}\mathrm{v_{bN}} + \boldsymbol{a}^2\mathrm{v_{cN}}) \tag{3}$$

where $\boldsymbol{a} = e^{j2\pi/3}$. The output voltage vector can be related to the switching combination as:

$$\boldsymbol{V_c} = \sqrt{\frac{2}{3}} V_{dc}(s_a + \boldsymbol{a}s_b + \boldsymbol{a}^2 s_c) \tag{4}$$

The components of the vector $\boldsymbol{V}_c$, in the orthogonal coordinate system $\alpha\beta$, are given as:

$$\begin{bmatrix} v_{c\alpha} \\ v_{c\beta} \end{bmatrix} = \begin{bmatrix} \frac{V_{dc}}{\sqrt{6}} & 0 \\ 0 & \frac{V_{dc}}{\sqrt{2}} \end{bmatrix} \begin{bmatrix} m_\alpha \\ n_\beta \end{bmatrix} \tag{5}$$

where m_α and n_β are both integers which are calculated by,

$$\begin{bmatrix} m_\alpha \\ n_\beta \end{bmatrix} = \begin{bmatrix} 2 & -1 & -1 \\ 0 & 1 & -1 \end{bmatrix} \begin{bmatrix} s_a \\ s_b \\ s_c \end{bmatrix} \tag{6}$$

Assuming a resistive-inductive model for the smoothing reactances of CHB STATCOM shown in Fig. 1, the STATCOM current dynamics can be described by,

$$\boldsymbol{V_s} = r\boldsymbol{i} + L\frac{d\boldsymbol{i}}{dt} + \boldsymbol{V_c} \tag{7}$$

where r and L are the resistance and inductance of the smoothing reactances, and $\boldsymbol{i}$, $\boldsymbol{V_s}$ are the STATCOM current and grid voltage space vectors, respectively. Therefore, the state space equations of the STATCOM will be,

$$\begin{bmatrix} \frac{di_\alpha}{dt} \\ \frac{di_\beta}{dt} \end{bmatrix} = \begin{bmatrix} -rL^{-1} & 0 \\ 0 & -rL^{-1} \end{bmatrix} \begin{bmatrix} i_\alpha \\ i_\beta \end{bmatrix} + \begin{bmatrix} -L^{-1} & 0 \\ 0 & -L^{-1} \end{bmatrix} \begin{bmatrix} v_{c\alpha} \\ v_{c\beta} \end{bmatrix} + \begin{bmatrix} L^{-1} & 0 \\ 0 & L^{-1} \end{bmatrix} \begin{bmatrix} v_{s\alpha} \\ v_{s\beta} \end{bmatrix}. \tag{8}$$

By replacing (5) into (8), the following state space equations are obtained for the converter:

$$\begin{bmatrix} \frac{di_\alpha}{dt} \\ \frac{di_\beta}{dt} \end{bmatrix} = \begin{bmatrix} -rL^{-1} & 0 \\ 0 & -rL^{-1} \end{bmatrix} \begin{bmatrix} i_\alpha \\ i_\beta \end{bmatrix} + \begin{bmatrix} \frac{-V_{dc}}{\sqrt{6}L} & 0 \\ 0 & \frac{-V_{dc}}{\sqrt{2}L} \end{bmatrix} \begin{bmatrix} m_\alpha \\ n_\beta \end{bmatrix} + \begin{bmatrix} L^{-1} & 0 \\ 0 & L^{-1} \end{bmatrix} \begin{bmatrix} v_{s\alpha} \\ v_{s\beta} \end{bmatrix}. \tag{9}$$

By substituting (6) into (9), the subsequent state space equations are resulted for the CHB STATCOM, where the input is the switching combination:

$$\begin{bmatrix} \frac{di_\alpha}{dt} \\ \frac{di_\beta}{dt} \end{bmatrix} = \begin{bmatrix} -rL^{-1} & 0 \\ 0 & -rL^{-1} \end{bmatrix} \begin{bmatrix} i_\alpha \\ i_\beta \end{bmatrix} + \begin{bmatrix} \frac{-2V_{dc}}{\sqrt{6}L} & \frac{-V_{dc}}{\sqrt{6}L} & \frac{-V_{dc}}{\sqrt{6}L} \\ 0 & \frac{-V_{dc}}{\sqrt{2}L} & \frac{-V_{dc}}{\sqrt{2}L} \end{bmatrix} \begin{bmatrix} s_a \\ s_b \\ s_c \end{bmatrix} + \begin{bmatrix} L^{-1} & 0 \\ 0 & L^{-1} \end{bmatrix} \begin{bmatrix} v_{s\alpha} \\ v_{s\beta} \end{bmatrix}. \tag{10}$$

Due to input redundancy in the state space equations (10), there is no unique solution for the switching combination, when the required output currents are known.

B. Proposed MPC Algorithm

The state space model of the multilevel converter is given by,

$$\dot{\boldsymbol{x}}(t) = \boldsymbol{A}\boldsymbol{x}(t) + \boldsymbol{B}\boldsymbol{u}(t) + \boldsymbol{E}\boldsymbol{d}(t) \tag{11}$$

where $\boldsymbol{x}(t)$ are the state variables, $\boldsymbol{u}(t)$ are the inputs, and $\boldsymbol{d}(t)$ are the disturbances. The matrices $\boldsymbol{A}$, $\boldsymbol{B}$, and $\boldsymbol{E}$ are nonsingular matrices, describing the system dynamic. The discrete time model of the converter is also given by:

$$\boldsymbol{x}(k+1) = \boldsymbol{A_d}\boldsymbol{x}(k) + \boldsymbol{B_d}\boldsymbol{u}(k) + \boldsymbol{E_d}\boldsymbol{d}(k) \quad (12)$$

where,

$$\boldsymbol{A_d} = e^{\boldsymbol{A}T_s},$$
$$\boldsymbol{B_d} = \left(\int_0^{T_s} e^{\boldsymbol{A}T_s} d\tau\right)\boldsymbol{B} = \boldsymbol{A}^{-1}(e^{\boldsymbol{A}T_s} - \boldsymbol{I})\boldsymbol{B}$$
$$\boldsymbol{E_d} = \left(\int_0^{T_s} e^{\boldsymbol{A}T_s} d\tau\right)\boldsymbol{E} = \boldsymbol{A}^{-1}(e^{\boldsymbol{A}T_s} - \boldsymbol{I})\boldsymbol{E} \quad (13)$$

T_s is the sampling time, and $\boldsymbol{I}$ is the unit matrix. By using the first-order approximation $e^{\boldsymbol{A}T_s} \cong \boldsymbol{I} + \boldsymbol{A}T_s$, which is valid for the small sampling time T_s, the discrete time model can be approximated by:

$$\boldsymbol{x}(k+1) \cong (\boldsymbol{I} + T_s\boldsymbol{A})\boldsymbol{x}(k) + T_s\boldsymbol{B}\boldsymbol{u}(k) + T_s\boldsymbol{E}\boldsymbol{d}(k) \quad (14)$$

For the large sampling time, the second-order approximation $e^{\boldsymbol{A}T_s} \cong \boldsymbol{I} + \boldsymbol{A}T_s + 0.5(\boldsymbol{A}T_s)^2$ could be used, if necessary. An absolute cost function is used for optimization as follows:

$$J = |\boldsymbol{x}(k+1) - \boldsymbol{x}^*(k+1)| \quad (15)$$

where the state variables $\boldsymbol{x}(k+1)$ are predicted by (14) for each possible input $\boldsymbol{u}(k)$ and measured values $\boldsymbol{x}(k)$ and $\boldsymbol{d}(k)$. For high sampling rate $\boldsymbol{x}^*(k+1) \approx \boldsymbol{x}^*(k)$, otherwise for highly dynamics systems the second order Lagrange extrapolation can be used as [29]:

$$\boldsymbol{x}^*(k+1) \cong 3\boldsymbol{x}^*(k) - 3\boldsymbol{x}^*(k-1) + \boldsymbol{x}^*(k-2). \quad (16)$$

To minimize the cost function (15), it is necessary that:

$$\boldsymbol{x}(k+1) = \boldsymbol{x}^*(k+1) \quad (17)$$

Replacing (17) into (14), the required optimal input is calculated directly by:

$$\hat{\boldsymbol{u}} \cong \boldsymbol{B}^{-1}(-(T_s^{-1}\boldsymbol{I} + \boldsymbol{A})\boldsymbol{x}(k) + T_s^{-1}\boldsymbol{x}^*(k+1) - \boldsymbol{E}\boldsymbol{d}(k)) \quad (18)$$

and the MPC has to find the optimal possible input $\boldsymbol{u}^*$ closest to this optimal input, i.e. the MPC optimization loop needs to search over a set of inputs to find the optimal possible input $\boldsymbol{u}^*$, minimizing an error function such as:

$$E = |\boldsymbol{u} - \hat{\boldsymbol{u}}|. \quad (19)$$

The optimal possible input $\boldsymbol{u}^*$, according to (14), should be applied to the converter at the beginning of the same sample time k. This means at the start of each sampling time, measuring state variables and disturbances, as well as search for optimal possible input $\boldsymbol{u}^*$, should be carried out in a very short time compared to the sample time T_s.

Measurement of the state variables and disturbances in the multilevel converters is also time-consuming. This is due to large number of measuring signals, and implementation of a method to reduce the measurement noise; e.g., by taking an average of several successive measurements of a quantity. These measurements at the start of sampling time greatly affect the performance of the proposed MPC. Therefore, a solution to this problem is also proposed.

The state variables and disturbances can also be measured just before the start of each sampling time. To this end, the processor at each sampling time, after the main computation to realize the MPC algorithm, starts measuring the variables and updates them regularly. At the beginning of the next sampling time, the measurement is stopped and the last updates of the measured values are used for the next main computation.

Fig. 2 (b) shows the sequence of operations required for the sample time k. In the next section, a quick method to achieve optimal possible input, will be presented in the CHB converter.

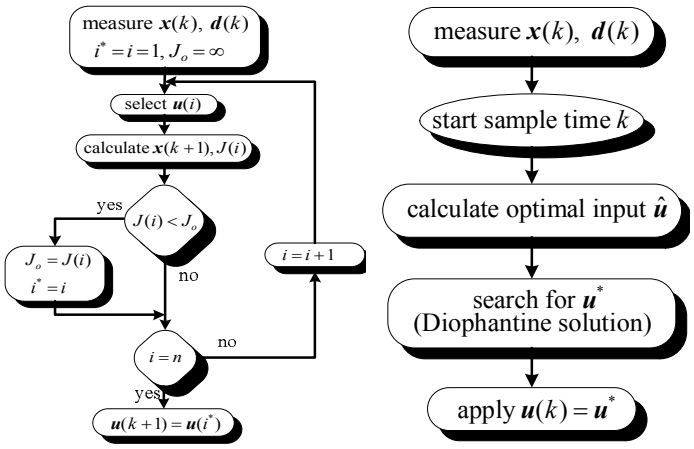

Fig. 2. MPC algorithms: (a) basic algorithm, (b) proposed algorithm.

C. Proposed MPC for CHB STATCOM

Due to an input redundancy variable in the system model (10), it cannot be used directly to implement the MPC algorithm. Therefore, the system model (9) is used for the converter CHB STATCOM. By replacing corresponding parameters into (18), the optimal input is obtained as:

$$\begin{bmatrix}\hat{m}_\alpha \\ \hat{n}_\beta\end{bmatrix} \cong \frac{1}{V_{dc}}\begin{bmatrix}\sqrt{6} & 0 \\ 0 & \sqrt{2}\end{bmatrix}\left((T_s^{-1}L - r)\begin{bmatrix}i_\alpha(k) \\ i_\beta(k)\end{bmatrix} - (T_s^{-1}L)\begin{bmatrix}i_\alpha^*(k+1) \\ i_\beta^*(k+1)\end{bmatrix} + \begin{bmatrix}v_{s\alpha}(k) \\ v_{s\beta}(k)\end{bmatrix}\right). \quad (20)$$

The optimal input vector $[\hat{s}_a\ \hat{s}_b\ \hat{s}_c]^T$ to the system model (10), may have several redundancies. It should be computed in $\mathbb{Z}$ domain (set of integers) for each optimal vector $[\hat{m}_\alpha\ \hat{n}_\beta]^T$ obtained from (20), by using (6) as:

$$\begin{bmatrix}2 & -1 & -1 \\ 0 & 1 & -1\end{bmatrix}\begin{bmatrix}\hat{s}_a \\ \hat{s}_b \\ \hat{s}_c\end{bmatrix} = \begin{bmatrix}\hat{m}_\alpha \\ \hat{n}_\beta\end{bmatrix} \quad (21)$$

constrained to:

$$\hat{s}_a,\ \hat{s}_b,\ \hat{s}_c \in [-N, N]. \quad (22)$$

Equation system (21) is called constrained system of Diophantine equations (here now temporarily assumed that $[\hat{m}_\alpha\ \hat{n}_\beta]^T \in \mathbb{Z}^2$). Several methods have been developed, determining whether there exists a solution for a given system of Diophantine equations in $\mathbb{Z}$ domain, and in case of existing solution(s), how to calculate all of them [25, 26]. Here a simple method is presented to solve (21). Summation of the two equations in the equations system (21) results:

$$\hat{s}_a - \hat{s}_c = \frac{1}{2}(\hat{m}_\alpha + \hat{n}_\beta) = \hat{k}_d \quad (23)$$

where $\hat{k}_d$ should be an integer due to $\hat{s}_a$ and $\hat{s}_c \in \mathbb{Z}$, i.e. for

solution(s) existence, both $\hat{m}_\alpha$ and $\hat{n}_\beta$ should be odd or even integers. It can be easily examined that one solution of (21) is $[\hat{k}_d\ \hat{n}_\beta\ 0]^T$, and also $[1\ 1\ 1]^T$ belongs to the null space of its coefficient matrix. Therefore, all solutions of (21) can be written as [26]:

$$\begin{bmatrix}\hat{s}_a\\ \hat{s}_b\\ \hat{s}_c\end{bmatrix}=\begin{bmatrix}\hat{k}_d\\ \hat{n}_\beta\\ 0\end{bmatrix}+\lambda\begin{bmatrix}1\\1\\1\end{bmatrix} \tag{24}$$

where $\lambda \in \mathbb{Z}$. The constraints (22) should be satisfied by (24). After applying those boundary values to relations $\hat{s}_a$, $\hat{s}_b$, $\hat{s}_c$ and solving the resulted unequally equations for parameter λ, their subscription yields:

$$\max(-N,-N-\hat{k}_d,-N-\hat{n}_\beta) \le \lambda \le \min(N,N-\hat{k}_d,N-\hat{n}_\beta) \tag{25}$$

All values of integer λ, satisfying unequally relation (25), can be replaced in (24) to generate an optimal switching combination and its redundancies. Therefore, total number of the switching combination and redundancies will be equal to $(\lambda_{max}-\lambda_{min}+1)$, where λ_{max} and λ_{min} are the max and min values of λ, respectively.

Table I shows some examples for different values of $[\hat{m}_\alpha\ \hat{n}_\beta]^T$ in a seven-cell CHB converter. In this table one of the switching combinations for λ_{min} is calculated by (24), and the number of redundancies, which can be calculated for other values of λ up to λ_{max} , are also listed.

As well as the switching combination, each of switching redundancies can be applied to the converter. The selection can be made according to a predefined strategy.

The proposed MPC algorithm can be summarized as follows:

1) The optimal control input $[\hat{m}_\alpha\ \hat{n}_\beta]^T$ is computed using (20).
2) The values of $\hat{k}_d$ and $\hat{n}_\beta$ are rounded to obtain optimal possible values k_d^* and n_β^*:

$$k_d^* = \text{round}\left(\frac{1}{2}(\hat{m}_\alpha+\hat{n}_\beta)\right) \tag{26}$$

$$n_\beta^* = \text{round}(\hat{n}_\beta) \tag{27}$$

The *round* function rounds its argument to the nearest integer.

3) The maximum and minimum values of λ are computed for k_d^* and n_β^* using (25), and an integer value in this range is selected, e.g. the mid value λ_{mid}. The selection can also be made to suit a particular purpose.
4) The optimal possible switching combination is obtained using (24), as follows:

$$\begin{bmatrix}s_a^*\\ s_b^*\\ s_c^*\end{bmatrix}=\begin{bmatrix}k_d^*\\ n_\beta^*\\ 0\end{bmatrix}+\lambda_{mid}\begin{bmatrix}1\\1\\1\end{bmatrix} \tag{28}$$

5) Switching combination $[s_a^*\ s_b^*\ s_c^*]^T$ is applied at sample time k, i.e.

$$\begin{bmatrix}s_a(k)\\ s_b(k)\\ s_c(k)\end{bmatrix}=\begin{bmatrix}s_a^*\\ s_b^*\\ s_c^*\end{bmatrix}. \tag{29}$$

The phase redundancies can be used to balance the associated dc links voltage of CHB STATCOM. In each sampling time k, if $i_a > 0$, then for $s_a(k) > 0$ the HBs with lower dc link voltages are placed in mode 1 up to $s_a(k)$ HBs (charging state), similarly for $s_a(k) < 0$ the HBs with higher dc link voltages are activated in mode -1 up to $|s_a(k)|$ HBs (discharging state). If $i_a < 0$, it should be carried out vice versa. The same method is applied to phases, b and c as well.

TABLE I
SOME CALCULATED SWITCHING COMBINATIONS FOR $N = 7$

$(\hat{m}_\alpha,\hat{n}_\beta)$	$\hat{k}_d$	λ_{min}	λ_{max}	$(\hat{s}_a,\hat{s}_b,\hat{s}_c)$ for λ_{min}	No. of Redun. $(\lambda_{max}$-$\lambda_{min})$
(28, 0)	14	-7	-7	(7, -7, -7)	0
(0, -2)	-1	-5	7	(-6, -7, -5)	12
(0, 0)	0	-7	7	(-7, -7, -7)	14
(3, 5)	4	-7	2	(-3, -2, -7)	9
(-3, -5)	-4	-2	7	(-6, -7, -2)	9
(-11, 13)	1	-7	-6	(-6, 6, -7)	1
(9, 7)	8	-7	-1	(1, 0, -7)	6

V. CHB STATCOM ESC

The proposed MPC algorithm is applied to a transformerless 15-level CHB STATCOM ESC, incorporating seven HB cells per phase at 20 kV. The CHB STATCOM ESC compensates the required reactive power of a 10 MW fixed speed wind farm, as well as smoothes short-term active power fluctuations due to tower shadow effects and wind gradient, known as 3p frequency oscillations. Power fluctuations with 3p frequency effectively impact on flicker emission of the wind farm [31, 32].

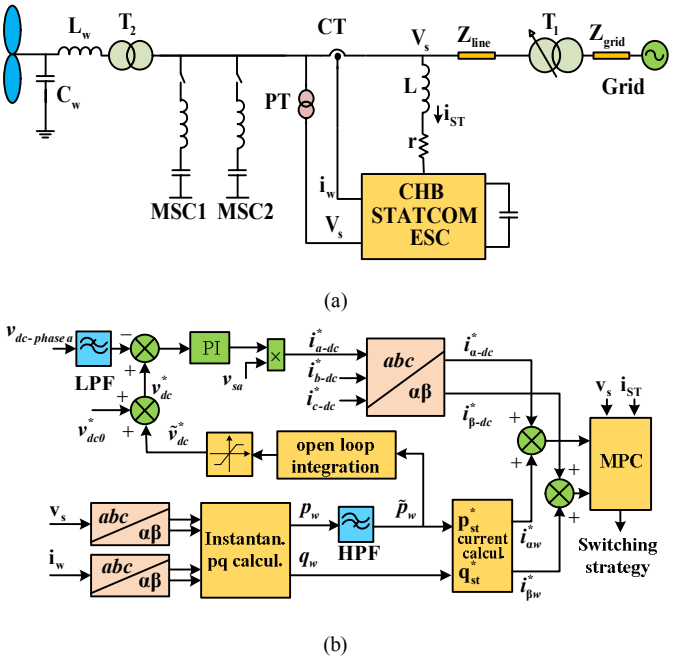

Fig. 3. Power system and control. (a) Single line diagram of the grid-connected wind farm, including CHB STATCOM ESC and MSCs. (b) CHB STATCOM ESC control block diagram.

A. CHB STATCOM ESC Specification

A 2 MVar, ±0.75 MW, 0.57 MJ CHB STATCOM ESC is connected to the Point of Common Coupling (PCC) of a grid connected fixed speed wind farm. Single line diagram of the power system is shown in Fig. 3 (a). The wind farm and the CHB STATCOM ESC specifications are given in Tables II and III of the appendix. The CHB STATCOM ESC can filter

out 3p frequency (1.3 Hz) of active power oscillations, by an outer control loop over the inner MPC loop, which charges and discharges the capacitors connected to the dc links. The converter can also compensate fluctuated var of the wind farm simultaneously up to 2 MVar. The remaining var is compensated by two 1.5 MVar Mechanical Switched Capacitors (MSC).

B. Control Block Diagram

The control block diagram of the CHB STATCOM ESC is shown in Fig. 3 (b). Based on the Instantaneous Power Theory (IPT), active power p_w and reactive power q_w are computed from the wind farm currents and voltages in the $\alpha\beta$ reference frame [33]. The active power is filtered through the high pass filter HPF with the cutoff frequency of 1.3 Hz (3p frequency), and the output $\tilde{p}_w$ along with the q_w are used to compute the current references $i^*_{\alpha w}$ and $i^*_{\beta w}$. The current references are calculated based on the IPT [33]. The dc bus voltage reference v^*_{dc} in Fig. 3 (b) for each phase, contains a constant component v^*_{dc0} and an oscillating component $\tilde{v}^*_{dc}$. The oscillating component, which is proportional to the energy changes of the capacitors of the dc links, can be calculated from the integral of the oscillatory power $\tilde{p}_w$. This task is performed by the block *open loop integration*, which is a low-pass filter with a proper gain and cutoff frequency. As shown in Fig. 3 (b), the dc voltage control loop of each phase contains a PI controller whose output is multiplied by the same phase voltage to provide a current signal in phase with the voltage signal. These current signals are transferred to the $\alpha\beta$ reference frame and the resulted currents are added with $i^*_{\alpha w}$ and $i^*_{\beta w}$ and transmitted as the current references to the MPC block. All of these pre-calculations are required to prepare the current references for the MPC at the start of each sampling time. In case of empirical implementation, these pre-calculations for each sampling time is done at about 0.55 µs by the processor used for this research.

VI. Simulation of the CHB STATCOM ESC

A. Square Wave Power Oscillation

The worst-case active power oscillations are the stepping changes. In this simulation, the active power is modulated by a 1.3 Hz, ±o.5 MW square wave. In Fig. 4, the CHB STATCOM ESC filters out the active power oscillations, and the variable reactive power is also compensated by the CHB STATCOM ESC and one of 1.5 MVar MSC.

B. Actual Power Fluctuation

An actual *12-second* active power generated by the fixed speed wind farm is fed into the grid for evaluation of the system performance in a realistic environment. Fig. 5 shows the short-term variations of the injected active power are eliminated, and the output active power tracks the average value of the input power coming from the wind farm.

C. Dynamic Performance

Dynamic performance of the MPC controlled STATCOM is demonstrated by applying a reactive power command change between zero up to 80% of rated value, whereas the command for variable component of active power is kept zero. Therefore, the command signal is just directly applied to the MPC and the dc bus command for charging, and discharging of dc link capacitors does not change. The dynamic response of the corresponding current for one phase is shown in Fig. 6. The output current tracks the input command after 2 ms.

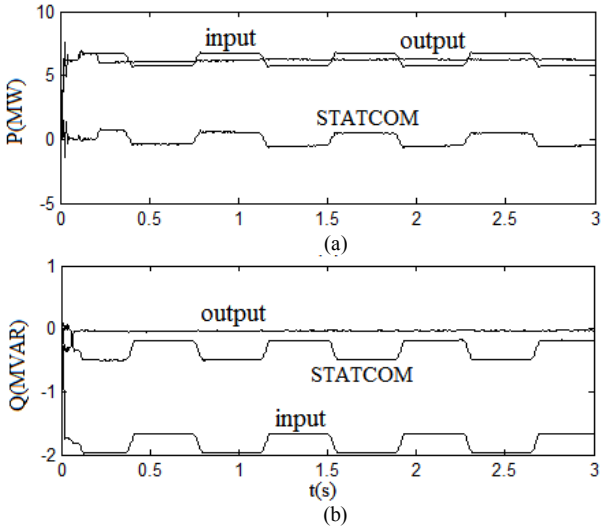

Fig. 4. Square wave oscillation of power. (a) Input, output to the grid, and STATCOM active powers. (b) Input, output to the grid, and STATCOM reactive powers.

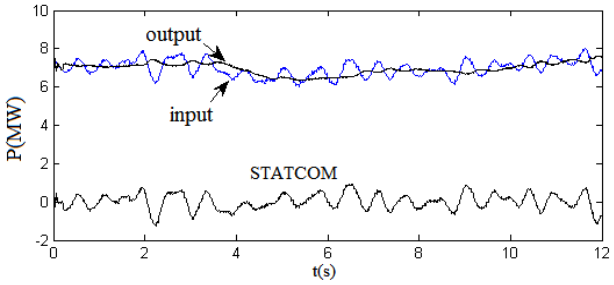

Fig. 5. 12-second active power profile of the wind farm (input), active power of the CHB STATCOM ESC, injected active power into the grid (output).

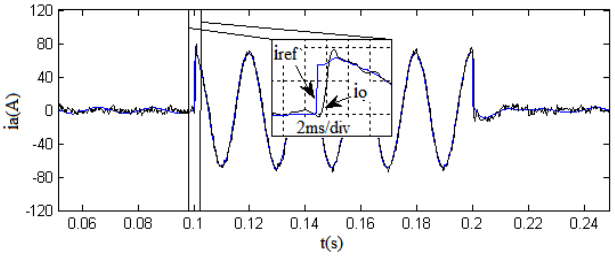

Fig. 6. MPC dynamic performance for reactive power step change of 80%. The reference and output currents of phase-A .

VII. CHB STATCOM Prototype

The proposed MPC algorithm is also applied to a laboratory prototype of 4 kVar transformerless 7-level CHB STATCOM with three HBs per phase at 380 V. Fig. 7 indicates the compensator while absorbing the rated reactive power from the network. The compensator specifications are given in Table IV of the appendix. The control algorithm is implemented using the processor STM32F429ZIT6U

This article has been accepted for publication in a future issue of this journal, but has not been fully edited. Content may change prior to final publication. Citation information: DOI 10.1109/TIE.2018.2833055, IEEE Transactions on Industrial Electronics

(180MHz) of the ST products. No need of relatively expensive DSP processors is the benefits of the proposed control algorithm. The DSP and FPGA are often used in the multilevel converters due to implementation complexities in the modulation schemes, large number of inputs and outputs, and sometimes the complex control method [6, 21, 23]. As mentioned earlier the proposed control approach, besides its simplicity, does not require any type of modulation methods.

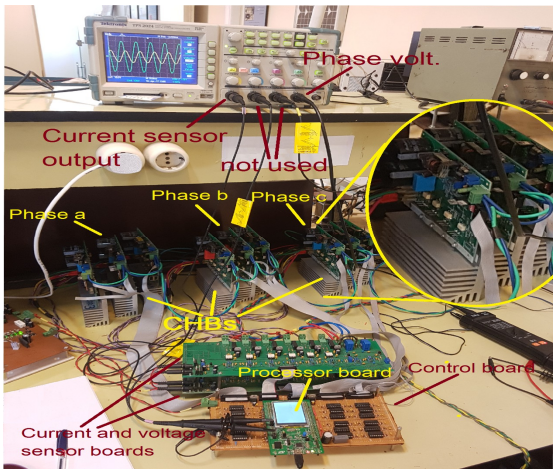

Fig. 7. Experimental setup

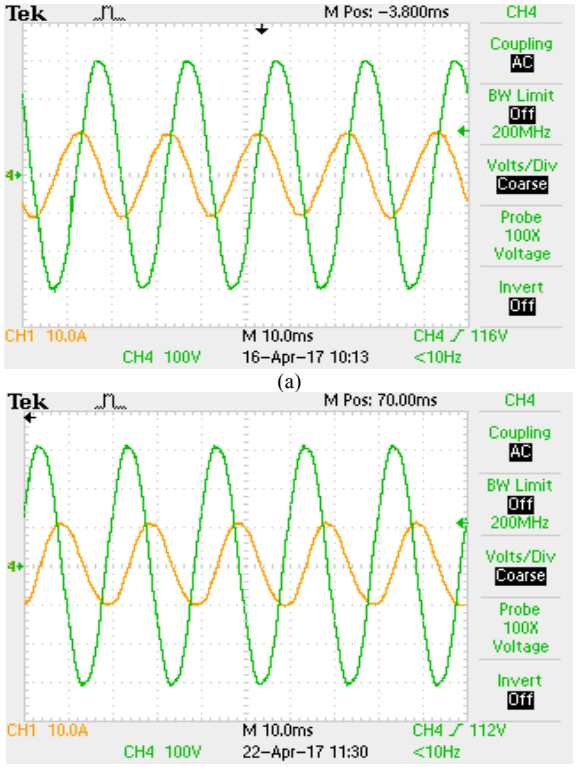

Fig. 8. Phase voltage (CH4) and phase current (CH1, $1.3i_a$) under the rated reactive power: (a) Capacitive mode. (b) Inductive mode.

VIII. Experimental Results

A. Experimental Waveforms

Fig. 8 illustrates the phase voltage and current waveforms under the rated reactive power (4 kVar) injection (capacitive mode) and absorption (inductive mode).

Fig. 9 depicts voltage waveforms of phase to inverter's neutral (v_{aN}), on the inverter shown in Fig. 1, line to line at the inverter side (v_{ll}), phase to grid's neutral (v_{an}) under the 50% capacitive and inductive modes. Due to the redundancies in the switching combinations, positive and negative half cycles of v_{aN} waveforms are not symmetrical; however, voltages v_{ll}, which are applied to the smoothing reactances of the compensator to create the three-phase currents, are symmetrical. In Fig. 9 (b), the voltage levels of v_{aN} and v_{ll} are decreased in the situation of reactive power absorption; consequently, the switching frequency is automatically increased to prevent an increase in the current error.

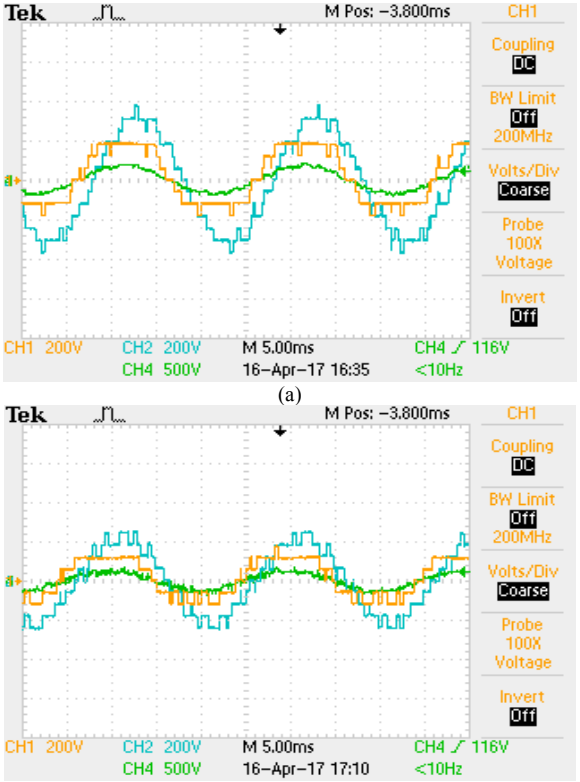

Fig. 9. Voltage waveforms of phase to neutral of the inverter (CH1, $0.5v_{aN}$), line to line (CH2, $0.5v_{ll}$), phase to neutral of grid (CH4, $0.5v_{an}$) under the 50% reactive power. (a) capacitive mode (b) inductive mode.

B. Dynamic Performance

The dynamic performance of the STATCOM is investigated by applying a reactive power step change command. In Fig. 10 (a), the reactive power command changes from capacitive mode (+80%) to inductive mode (-80%). The output phase current tracks the step change of reference current fairly well after about 3 ms.

Simplicity and fast computations of the proposed MPC provide the possibility of implementing it on a platform with a single processor. Implementation the proposed methods of [23] and [24] on the platform of this paper is hardly feasible, and similar to their own platform, the implementation requires FPGA with external ADCs and auxiliary microcontrollers. Fig. 10 (b) shows the dynamic performance of an MPC

This article has been accepted for publication in a future issue of this journal, but has not been fully edited. Content may change prior to final publication. Citation information: DOI 10.1109/TIE.2018.2833055, IEEE Transactions on Industrial Electronics

scheme, which is developed using the limited search subspace method in the platform of this paper [22]. The scheme restricts the search subspace of switching combinations, so that at the next sampling time, the voltage progression is possible only to an adjacent vector. The waveforms indicate that in the steady state, the output current tracks well the reference current. However, in the transient state, for a large instant change in the reference current, the output current is not fast enough. This is due to the output voltage of the converter could not change rapidly, for tracking a momentary and severe change of the current reference [21].

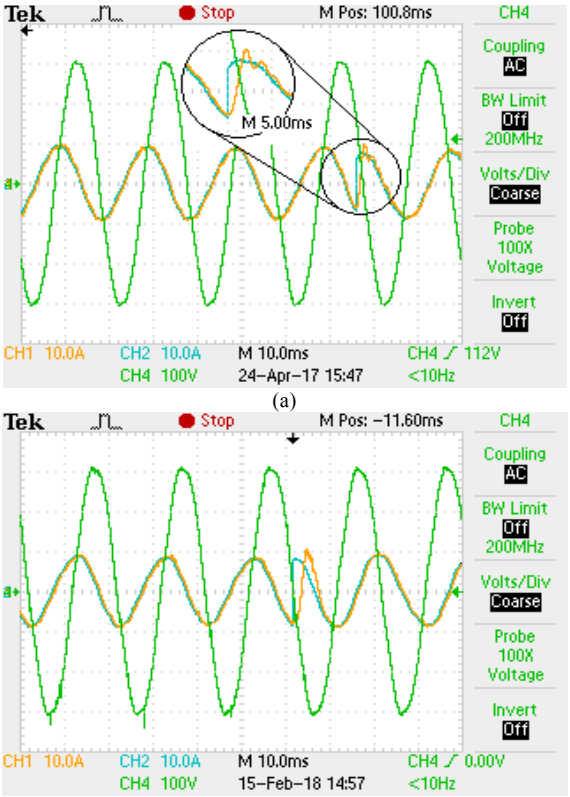

Fig. 10. Phase voltage (CH4), phase current (CH1, $1.3i_a$), phase current reference (CH2, $1.3i_{aref}$) waveforms under the +80% (capacitive) to -80% (inductive) reactive power step change: (a) proposed MPC (b) MPC scheme with the restricted search subspace.

C. Model Dependency

Given that the quality of MPC algorithm depends on the modeling accuracy of the system, the effect of modeling error in the modeling of inductance L, at 50% of rated reactive power is studied. The impact of uncertainty about the value of smoothing inductance, on the square of the effective value of the converter current error, is depicted in Fig. 11 (a). As it can be seen, underestimation has a deeper impact on increasing the current error. By contrast, overestimation slightly further reduces the error, however, leads to higher switching frequency. These effects can also be seen in Fig. 11 (b), illustrating current error waveforms under the three modeling errors +50%, 0, and -50%.

D. DC Links Voltage

In Fig. 12 dc link voltages of the first cells of the three phases, and the three cells of phase-A are shown at 50% reactive power injection. There is a 100 Hz low-amplitude ripple (6.5%) on each voltage; however, average values of them are equal. The dc link voltages of three cells of phase-A are completely balanced.

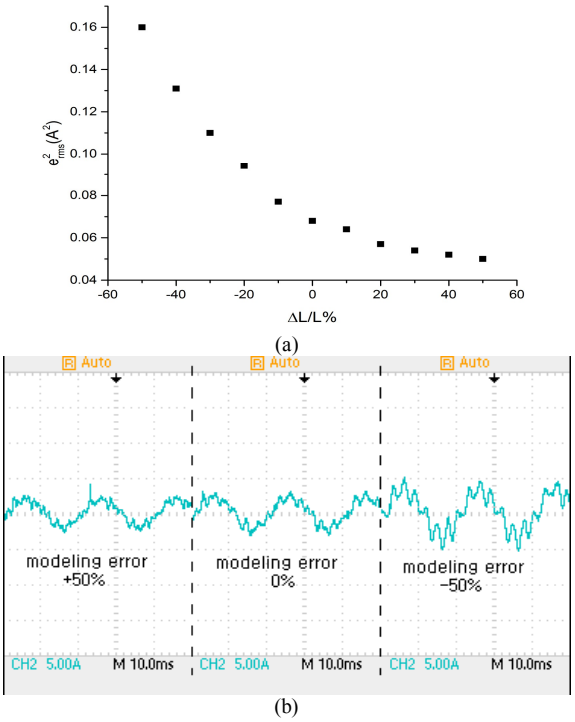

Fig. 11. (a) Effect of modeling error on the square of the effective value (rms) of the converter current error. (b) Current error waveforms (6.5 times larger) under the modeling errors +50%, 0%, and -50%.

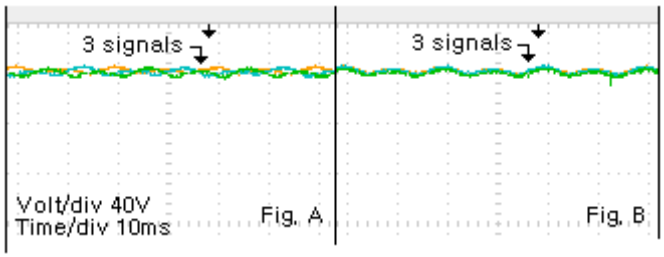

Fig. 12. dc link voltages of the first cells of the three phases (Fig. A), dc link voltages of the three cells of phase-A (Fig. B), STATCOM injects 50% reactive power.

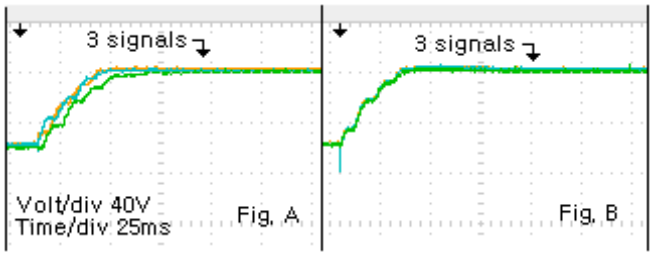

Fig. 13. Startup transient state, dc link voltages of the first cells of the three phases (Fig. A), dc link voltages of the three cells of phase-A (Fig. B).

Fig. 13 shows the same dc link voltages at the startup. The dc links are preliminary charged up to 50% by the reverse diodes of IGBTs (IGBTs are off), then the switching is started, and the dc link voltages reach to the rated values. The three dc

link voltages of different phases with little difference in the transient state, reach to the same rated value. The dc link voltages of phase-A are perfectly balanced.

IX. Conclusion

The MPC algorithm has been presented for the symmetrical multilevel converter control as a static var compensator. A large number of switching combinations and redundancies in these converters increase the optimization time of the MPC algorithm; therefore, the use of algorithm and enjoying its benefits has been faced with a major challenge. This paper replaced the time-consuming optimization loop of MPC algorithm, by direct solution of the system model and solving the system of Diophantine equations in the domain of integers on a large set of switching combinations to find the optimal possible input. At the start of each sampling time, the optimal possible switching combination and all its redundancies were provided in a minimum execution time. In the multilevel CHB converter with a high number of measuring data, A technique proposed for the data measurement, which also reduced effectively the MPC algorithm processing time, by eliminating the time required for measuring data from the start of each sampling time. Due to simplicity and no need to any modulation scheme, digital implementation of the proposed algorithm, did not require a relatively expensive processor like DSP or parallel processing units such as FPGAs, which are usually used for the CHB converters.

The algorithm was validated by simulation and experimental implementation for two seven-cell and three-cell CHB STATCOMs, respectively. The results showed that the proposed MPC algorithm exposes high dynamic performance to control the CHB STATCOM with any number of cells.

The Diophantine solution speeds up finding optimal switching combination in a multilevel converter, and allows all its redundancies to be generated in each sample time simply by changing an integer variable within a given range. Therefore, each objective function, defined to take advantages of these redundancies, can be easily optimized to obtain the optimal redundancy. The proposed scheme is applicable to the converters whose control signals are considered integers with many redundancies. However, the method will work more effective, If the converter is modeled so that the number of input variables to the model due to redundancy, is not much more than the number of output variables. This will lead to simpler Diophantine equations with less integer unknowns.

Appendix

Table II
Grid connected wind farm parameters

	power	volt.	resist.*	react.*	freq.
wind farm	10.34 MW	20 kV	-	-	
12Km feeder	-	20 kV	1.3136 Ω	3.9582 Ω	50 Hz
grid+trans.	200 MVA	20 kV	0.5373 Ω	3.2865 Ω	

* All parameters have been transferred to 20 kV side.

Table III
Parameters of the CHB STATCOM ESC

parameter	value	parameter	value
voltage	20 kV	ΔE	0.57 MJ
current	61.6 A	react. (5%)	9.3 Ω
Q	2 MVar	dc link volt.	3.22±0.778 kV
ΔP	±0.75 MW	C	5.5 mF

Table IV
Parameters of the CHB STATCOM prototype

parameter	value	parameter	value
voltage	380 V	react. (20%)	7.22 Ω
current	6.06 A	dc link volt.	120 V
Q	4 kVar	C	2 mF

References

[1] Q. Song, W. Liu, and Z. Yuan, "Multilevel optimal modulation and dynamic control strategies for STATCOMs using cascaded multilevel inverters," *IEEE trans. power del.,* vol. 22, no. 3, pp. 1937-1946, 2007.

[2] M. Malinowski, K. Gopakumar, J. Rodriguez, and M. A. Perez, "A survey on cascaded multilevel inverters," *IEEE Trans. Indust. Elect.,* vol. 57, no. 7, pp. 2197-2206, 2010.

[3] J. Muñoz, J. Rohten, J. Espinoza, P. Melín, C. Baier, and M. Rivera, "Review of current control techniques for a cascaded H-Bridge STATCOM," in *Indust. Tech. (ICIT), IEEE Inter. Conf.*, pp. 3085-3090, 2015.

[4] J. Vivas, G. Bergna, and M. Boyra, "Comparison of multilevel converter-based STATCOMs," in *Power Elect. and App. (EPE 2011)*, pp. 1-10, 2011.

[5] G. Farivar, B. Hredzak, and V. G. Agelidis, "Decoupled control system for cascaded H-bridge multilevel converter based STATCOM," *IEEE Trans. Indust. Elect.,* vol. 63, no. 1, pp. 322-331, 2016.

[6] C. D. Townsend, T. J. Summers, and R. E. Betz, "Phase-shifted carrier modulation techniques for cascaded H-bridge multilevel converters," *IEEE Trans. Indust. Elect.,* vol. 62, no. 11, pp. 6684-6696, 2015.

[7] L. K. Haw, M. S. Dahidah, and H. A. Almurib, "A new reactive current reference algorithm for the STATCOM system based on cascaded multilevel inverters," *IEEE Trans. power elect.,* vol. 30, no. 7, pp. 3577-3588, 2015.

[8] D. Q. Mayne, "Model predictive control: Recent developments and future promise," *Automatica,* vol. 50, no. 12, pp. 2967-2986, 2014.

[9] S. Kouro, P. Cortés, R. Vargas, U. Ammann, and J. Rodríguez, "Model predictive control—A simple and powerful method to control power converters," *IEEE Trans. Indust. Elec.,* vol. 56, no. 6, pp. 1826-1838, 2009.

[10] S. Vazquez, J. Rodriguez, M. Rivera, L. G. Franquelo, and M. Norambuena, "Model predictive control for power converters and drives: Advances and trends," *IEEE Trans. Indust. Elect.,* vol. 64, no. 2, pp. 935-947, 2017.

[11] C. Bordons and C. Montero, "Basic principles of MPC for power converters: Bridging the gap between theory and practice," *IEEE Indust. Elect. Mag.,* vol. 9, no. 3, pp. 31-43, 2015.

[12] G. A. Papafotiou, G. D. Demetriades, and V. G. Agelidis, "Technology readiness assessment of model predictive control in medium-and high-voltage power electronics," *IEEE Trans. Indust. Elect.,* vol. 63, no. 9, pp. 5807-5815, 2016.

[13] S. Vazquez, J. I. Leon, L. G. Franquelo, J. Rodriguez, H. A. Young, A. Marquez, and P. Zanchetta, "Model predictive control: A review of its applications in power electronics," *IEEE Indust. Elect. Mag.,* vol. 8, no. 1, pp. 16-31, 2014.

[14] J. Rodriguez, M. P. Kazmierkowski, J. R. Espinoza, P. Zanchetta, H. Abu-Rub, H. A. Young, and C. A. Rojas, "State of the art of finite control set model predictive control in power electronics," *IEEE Trans. on Indus. Inform.,* vol. 9, no. 2, pp. 1003-1016, 2013.

[15] P. Cortes, J. Rodriguez, C. Silva, and A. Flores, "Delay compensation in model predictive current control of a three-phase inverter," *IEEE Trans. Indust. Elect.,* vol. 59, no. 2, pp. 1323-1325, 2012.

[16] A. Darba, F. De Belie, P. D'haese, and J. A. Melkebeek, "Improved dynamic behavior in BLDC drives using model predictive speed and current control," *IEEE Trans. Indust. Elect.,* vol. 63, no. 2, pp. 728-740, 2016.

[17] L. Tarisciotti, P. Zanchetta, A. Watson, P. Wheeler, J. C. Clare, and S. Bifaretti, "Multiobjective modulated model predictive control for a multilevel solid-state transformer," *IEEE Trans. Industry App.,* vol. 51, no. 5, pp. 4051-4060, 2015.

[18] M. Narimani, B. Wu, V. Yaramasu, Z. Cheng, and N. R. Zargari, "Finite control-set model predictive control (FCS-MPC) of nested neutral point-clamped (NNPC) converter," *IEEE Trans. power elect.,* vol. 30, no. 12, pp. 7262-7269, 2015.

[19] A. Formentini, A. Trentin, M. Marchesoni, P. Zanchetta, and P. Wheeler, "Speed finite control set model predictive control of a PMSM fed by matrix converter," *IEEE Trans. Indust. Elect.,* vol. 62, no. 11, pp. 6786-6796, 2015.

[20] V. Yaramasu and B. Wu, "Predictive control of a three-level boost converter and an NPC inverter for high-power PMSG-based medium voltage wind energy conversion systems," *IEEE Trans. power elect.,* vol. 29, no. 10, pp. 5308-5322, 2014.

[21] C. D. Townsend, T. J. Summers, and R. E. Betz, "Multigoal heuristic model predictive control technique applied to a cascaded H-bridge StatCom," *IEEE Trans. power elect.,* vol. 27, no. 3, pp. 1191-1200, 2012.

[22] P. Cortes, A. Wilson, S. Kouro, J. Rodriguez, and H. Abu-Rub, "Model predictive control of multilevel cascaded H-bridge inverters," *IEEE Trans. Indust. Elect.,* vol. 57, no. 8, pp. 2691-2699, 2010.

[23] Y. Zhang, X. Wu, X. Yuan, Y. Wang, and P. Dai, "Fast model predictive control for multilevel cascaded H-bridge STATCOM with polynomial computation time," *IEEE Trans. Indust. Elect.,* vol. 63, no. 8, pp. 5231-5243, 2016.

[24] Y. Zhang, X. Wu, and X. Yuan, "A Simplified Branch and Bound Approach for Model Predictive Control of Multilevel Cascaded H-Bridge STATCOM," *IEEE Trans. Indust. Elect.,* vol. 64, no. 10, pp. 7634-7644, 2017.

[25] M. Khorramizadeh and N. Mahdavi-Amiri, "On solving linear Diophantine systems using generalized Rosser's algorithm," *Iranian Math. Soci. Bulletin,* vol. 34, pp. 1-25, 2011.

[26] K. Aardal, C. A. Hurkens, and A. K. Lenstra, "Solving a system of linear diophantine equations with lower and upper bounds on the variables," *Operations Research Math.,* vol. 25, no. 3, pp. 427-442, 2000.

[27] B. Wu and M. Narimani, *High-power converters and AC drives*: John Wiley & Sons, 2017.

[28] M. A. Pérez, P. Cortés, and J. Rodríguez, "Predictive control algorithm technique for multilevel asymmetric cascaded H-bridge inverters," *IEEE Trans. Indust. Elec.,* vol. 55, no. 12, pp. 4354-4361, 2008.

[29] J. Rodríguez, J. Pontt, C. A. Silva, P. Correa, P. Lezana, P. Cortés, and U. Ammann, "Predictive current control of a voltage source inverter," *IEEE Trans. Indust. Elec.,* vol. 54, no. 1, pp. 495-503, 2007.

[30] E. Behrouzian, "Operation and control of cascaded H-bridge converter for STATCOM application," PhD thesis, Chalmers University of Technology, 2016.

[31] M. Rahimi and H. Assari, "Addressing and assessing the issues related to connection of the wind turbine generators to the distribution grid," *International Journal of Elect. Power & Energy Syst.,* vol. 86, pp. 138-153, 2017.

[32] W. Hu, Z. Chen, Y. Wang, and Z. Wang, "Flicker mitigation by active power control of variable-speed wind turbines with full-scale back-to-back power converters," *IEEE Trans. Energy conv.,* vol. 24, no. 3, pp. 640-649, 2009.

[33] H. Akagi, E. H. Watanabe, and M. Aredes, *Instantaneous power theory and applications to power conditioning* vol. 62: John Wiley & Sons, 2017.

Mohammad Reza Nasiri received B.Sc. degree in electronic engineering with honors from Amirkabir University, Tehran, Iran, in 1997, and M.Sc. degree in electrical engineering with honors from Sharif University, Tehran, Iran, in 1999. He is currently a PhD Candidate at the department of Electrical and Computer Engineering, Tehran University, Tehran, Iran. His research interests include design, modeling, and control of power electronic converters by applying control methods such as predictive control, hybrid predictive-repetitive control, sliding mode control and neural networks. He is also active in renewable energy and power quality improvement areas as well as short-term energy storage systems for renewable-energy applications.

Shahrokh Farhangi (M'90) obtained the B.Sc., M.Sc and Ph.D. degrees in electrical engineering from University of Tehran, Iran, with honors. He is currently professor of School of Electrical and Computer Engineering, University of Tehran. His research interests include design and modeling of Power Electronic Converters, Drives, Photovoltaics and Renewable Energy Systems. He has published more than 100 papers in conference proceedings and journals. He has managed several research and industrial projects, which some of them have won national and international awards. He has been selected as the distinguished engineer in electrical engineering by Iran Academy of Sciences, in 2008.

Jose Rodriguez (M'81-SM'94-F'10) received the Engineer degree in electrical engineering from the Universidad Tecnica Federico Santa Maria, in Valparaiso, Chile, in 1977 and the Dr.-Ing. degree in electrical engineering from the University of Erlangen, Erlangen, Germany, in 1985. He has been with the Department of Electronics Engineering, Universidad Tecnica Federico Santa Maria, since 1977. Since 2015 he is the President of Universidad Andres Bello in Santiago, Chile. He has coauthored two books, several book chapters and more than 400 journal and conference papers. His research interests include multilevel inverters, new converter topologies, control of power converters, and adjustable-speed drives. He has received a number of best paper awards from journals of the IEEE. Dr. Rodriguez is member of the Chilean Academy of Engineering. In 2014 he received the National Award of Applied Sciences and Technology of Chile. In 2015 he received the Eugene Mittelmann Award from the IES.